Contact stiffness of layered materials for ultrasonic atomic force microscopy

G. G. Yaralioglu,[a] F. L. Degertekin, K. B. Crozier, and C. F. Quate
Ginzton Laboratory, Stanford University, Stanford, California 94305

(Received 18 November 1999; accepted for publication 4 February 2000)

A method to calculate the contact stiffness between a layered material and an ultrasonic atomic force microscope (UAFM) tip is proposed. The radiation impedance method is used to determine the ratio of the applied force to the average displacement within the contact area. This information is used in an iterative algorithm based on Hertzian theory to obtain the contact stiffness. The algorithm converges into a couple of iterations and does not suffer from numerical convergence difficulties as does finite element analysis (FEA). In the ultrasonic frequency range, comparisons with Hertzian theory and FEA show the validity of the results in a quasistatic case. Definitions of the minimum detectable layer thickness and the penetration depth of the UAFM are given and evaluated for several thin film–substrate pairs. These results also show the potential of the method for modeling defects and power loss due to radiation in layered materials. © *2000 American Institute of Physics.* [S0021-8979(00)01110-5]

I. INTRODUCTION

Dynamic implementations of the atomic force microscope (AFM)[1] turn this device into a powerful material characterization tool. Ultrasonic methods like atomic force acoustic microscopy (AFAM),[2] scanning microdeformation microscopy (SMM),[3] and ultrasonic force microscopy (UFM)[4] enable high resolution measurement of the local elasticity of material surfaces. In all of the above methods, high order flexural or torsional modes of the cantilever are excited by vibrating the cantilever or the sample. The cantilever vibration is then detected by optical means. The dc force on the cantilever is adjusted to maintain continuous contact between the AFM tip and the sample. The contact mechanics shift the resonance frequencies of the cantilever. By detecting these shifts, the tip–sample contact stiffness is measured and, with Hertzian theory, material properties such as the Young's modulus are calculated.[5,6] Ultrasonic AFM can be used to determine the layer thickness through the stiffness measurement with high lateral resolution. Our aim here was to develop a theoretical model for analyzing the effect of thin films on the response of an ultrasonic AFM and investigate its thin film measurement ability.

The contact problem between two elastic half spaces was first solved analytically by Hertz.[7] By using the theory of elasticity, it is possible to generalize his results to include layered materials. However, an analytical solution is difficult to obtain for the layered case, especially for multilayered materials. On the other hand, numerical methods like finite element analysis (FEA) encounter convergence difficulties because a nonlinear analysis is required and typically the computation time is excessive. Moreover, both the analytical approach and FEA are valid only under quasistatic assumptions.

[a]Electronic mail: goksenin@leland.stanford.edu

In this article, Hertzian theory and the radiation impedance method[8,9] are combined to calculate the contact mechanics between an AFM tip and a layered material. In Sec. II, the radiation impedance method is described and its relation to the equivalent surface stiffness is established. An iterative algorithm which combines the results of the radiation impedance method and Hertzian contact theory is then presented. The results of the algorithm for half spaces and layered materials are compared with Hertzian theory and FEA, respectively, for the quasistatic case. The penetration depth and thin film thickness sensitivity of the ultrasonic AFM are discussed before our concluding remarks.

II. RADIATION IMPEDANCE METHOD FOR CALCULATION OF SURFACE STIFFNESS

When a vibrating AFM cantilever is brought into contact with a flat surface by a dc force, the AFM tip–surface contact will form a finite size ultrasonic source radiating into the surface as depicted in Fig 1. If the cantilever vibration is of a flexural nature, the traction applied to the surface will be predominantly in the direction of the surface normal. For a spherical tip geometry, the source will be circular with a contact radius a_S. Assuming that this contact radius is know, one can calculate the effective radiation impedance seen by the tip. For cases when $a_S \ll \lambda_m$, where λ_m is the smallest wavelength in the probed solid at the vibration frequency, the quasistatic approximation can be used. This allows one to approximate the mechanical impedance by a lumped spring element and the effective stiffness of the surface can be obtained. As expected, the results of this method converge to the Hertzian contact approximation in the quasistatic case. Furthermore, the radiation impedance method can be used to find the effects of layers and high operating frequencies on tip–sample interaction which cannot be analyzed by static methods.

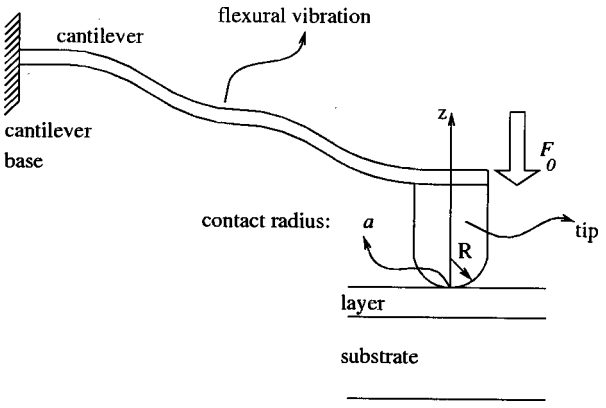

FIG. 1. Ultrasonic AFM cantilever. The tip is kept in contact with a layered half space by the dc force F_0.

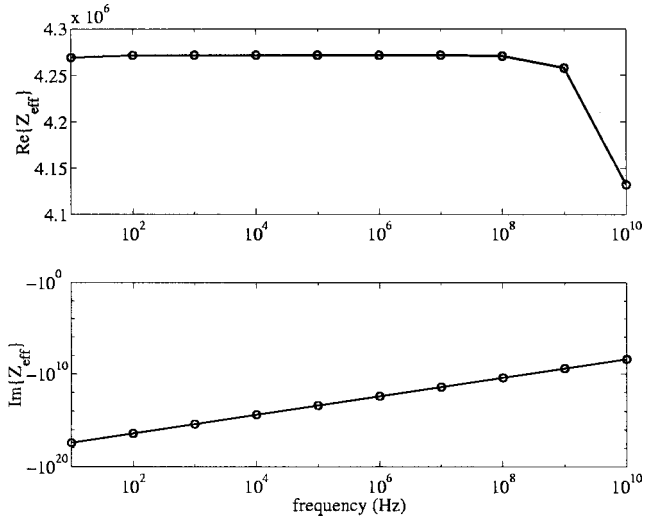

FIG. 2. Radiation impedance, Z_{eff}, of a silicon half space for a source with a 5 nm contact radius (arb units).

The problem of radiation impedance of mechanical radiators on a free half space has been studied by several investigators.[8,9] The calculation method that will be used here is based on a variational expression derived for ultrasonic transducers attached to an isotropic half space.[8] Given a normal stress distribution $T_{zz}(x,y)$ over a region S at the surface of a solid half space and a normal particle velocity distribution $v_z(x,y)$ due this surface stress source, the effective radiation impedance, Z_{eff}, is defined by the relation,

$$\frac{1}{Z_{\text{eff}}}=\frac{-\int\int_S T_{zz}^*(x,y)v_z(x,y)dxdy}{\int\int_S T_{zz}(x,y)T_{zz}^*(x,y)dxdy}. \tag{2.1}$$

Using the analogy that voltage and current in a circuit are a dual between stress and particle velocity, respectively, this expression can be understood as the ratio of the complex power to the magnitude of the applied voltage squared. In order to use plane wave solutions to find Z_{eff} in a problem with circular symmetry, the Parseval relation can be used to rewrite Eq. (2.1) in the Fourier transform domain as

$$\frac{1}{Z_{\text{eff}}}=\frac{-\int_0^\infty \mathcal{T}_{zz}^*(k_r)\mathcal{V}_z(k_r)k_r dk_r}{\int_0^\infty |\mathcal{T}_{zz}(k_r)|^2 k_r dk_r}, \tag{2.2}$$

where k_r is the radial wave number.

For AFM tip–surface contact, it is assumed that the tip applies uniform stress of unit magnitude over the contact area. In this case, $\mathcal{F}\{T_{zz}(x,y)\}=\mathcal{T}_{zz}(k_r)=2\pi a[J_1(k_r a)/k_r]$, where $\mathcal{F}\{\cdot\}$ denotes the Fourier transform and $J_1(\cdot)$ is the Bessel function of the first kind, order one. At this point, the effective radiation impedance of any solid medium at the surface can be evaluated if the relation between a normal stress plane wave and the resulting normal particle velocity is known. The surface impedance tensor provides this relation for solids with arbitrary laycring and material properties. It relates the stress components $\mathcal{T}_{xz}$, $\mathcal{T}_{yz}$, $\mathcal{T}_{zz}$ on a plane with its normal in the z direction to the particle velocity fields.[10,11] Hence the surface impedance tensor $\mathbf{G}(k_l,z)$ is defined as

$$\begin{bmatrix}\mathcal{T}_{xz}(k_l)\\ \mathcal{T}_{yz}(k_l)\\ \mathcal{T}_{zz}(k_l)\end{bmatrix}=\mathbf{G}(k_l,z)\begin{bmatrix}\mathcal{V}_x(k_l)\\ \mathcal{V}_y(k_l)\\ \mathcal{V}_z(k_l)\end{bmatrix}, \tag{2.3}$$

where k_l is the lateral wave number of the plane wave and z dependence is assumed for the particle velocity and stress fields. Details of the surface impedance tensor calculation for layered materials can be found elsewhere.[10–12] With the assumption that only T_{zz} of unit amplitude is applied to the surface by the AFM tip, the expression for the radiation impedance of the solid medium takes its final form,

$$\frac{1}{Z_{\text{eff}}}=-\frac{2\pi a_S^2\int_0^\infty |[J_1(k_r a_S)/k_r]|^2\mathbf{G}_{3,3}^{-1}(k_r)k_r dk_r}{\pi a_S^2}$$

$$=-2\int_0^\infty |[J_1(k_r a_S)/k_r]|^2\mathbf{G}_{3,3}^{-1}(k_r)k_r dk_r, \tag{2.4}$$

where $z=0$ and $\mathbf{G}_{3,3}^{-1}(k_r)$ denotes the scalar element with index (3,3) in the inverse of the surface impedance tensor matrix.

As an example, Eq. (2.4) is used to calculate the effective radiation impedance of a silicon half space assuming a contact radius of 5 nm, which is typical in AFM applications. The result, shown in Fig. 2, suggests that the medium presents mostly a reactive load to the tip in the frequency range up to 10 GHz and very small radiation loss. It also shows that the surface stiffness can be safely modeled by a lumped spring element. To obtain the spring constant, the normal force applied on the contact should be divided by the average surface displacement. Hence, the spring constant, k_S, which represents the surface stiffness is given by

$$k_S=\frac{\text{normal force on contact}}{\text{displacement}}=j\omega Z_S=j\omega A Z_{\text{eff}}, \tag{2.5}$$

where Z_S is the mechanical impedance, ω is the angular frequency, and A is the contact area. Note that k_S has both real and imaginary parts since the radiation impedance is complex.

III. CONTACT STIFFNESS CALCULATION ALGORITHM

The surface stiffness calculation presented in Sec. II does not consider deformation of the tip. However, to obtain

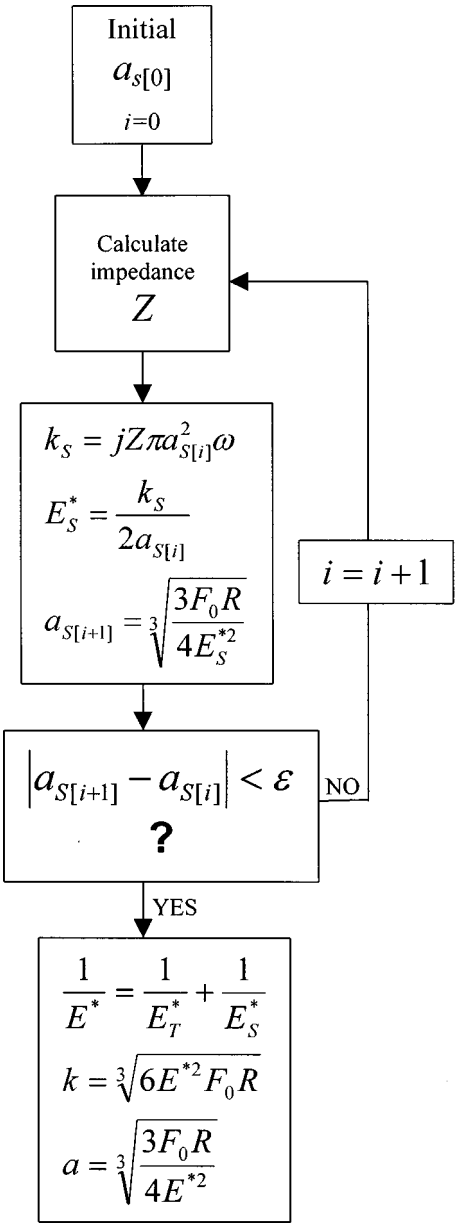

FIG. 3. Contact stiffness algorithm. ϵ in the decision box shows the accuracy of the convergence. The algorithm converges into three or four iterations with a relative accuracy of 0.1%.

contact stiffness, the finite stiffness of the tip should also be included in the analysis. Tip deformation is dictated by the material properties and by the radius of curvature of the tip, R, as well as by the force between the tip and the surface, F_0. To include these factors, an iterative algorithm combining Hertzian theory and the radiation impedance method is proposed. The contact stiffness algorithm (CSA), depicted in Fig. 3, calculates an effective reduced Young's modulus, E_S^*, for the layered surface iterating on the contact radius and assuming a rigid intruder. At each step, the surface stiffness is calculated using the radiation impedance method. Hertzian theory is used to relate the contact radius, a_S, to the spring constant, k_S, and the contact radius is updated until it converges within error limits. Once a_S converges, the surface can be treated as a half space with reduced Young's modulus E_S^*. The contact radius, a, and the spring constant, k, can then be calculated using Hertzian theory as outlined in the Appendix.

The algorithm converges into three or four iterations if initial estimates for the a_S are obtained by making half space approximations.

TABLE I. Material constants used in the calculations.

Material	Young's modulus (GPa)	Poisson's ratio	Density (kg/cm^3)
Silicon	130.10	0.2780	2332.0
Aluminum	66.995	0.3564	2700.0
Photoresist	3.7151	0.3712	1120.0
Tungsten	361.83	0.4378	19 200.0

IV. RESULTS AND DISCUSSION

A comparative study has to be performed to test the validity of the CSA. For layered materials, Hertzian theory does not provide an analytical solution. Hence, the results of the CSA can only be compared to the FEA results. On the other hand, for half spaces an analytical solution exists and it can be used to verify both FEA and the CSA.

A. Verification of CSA for half spaces

Three methods are tested on half space materials with a wide range of stiffness, such as photoresist, aluminum, silicon, and tungsten (see Table I).[13] Silicon is chosen as the tip material. The force, F_0, and the radius of curvature of the tip, R, are set to 200 nN and 100 nm, respectively. Analytical values of the contact radius and stiffness are obtained using Eqs. (A1) and (A2) which are the results of Hertzian contact theory.

The FEA calculations are carried out using ANSYS5.5.[14] The tip and the sample are meshed with axisymmetric two dimensional (2D) structural finite elements (PLANE42). The mesh in the possible interaction area is overlaid by surface-to-surface contact elements (TARGE169, CONTA172). Then, nonlinear static analysis[15] is performed. The contact radius is determined by the location of the outermost contacting node from the center of the contact. Hence, the accuracy of the contact radius calculation is determined by the size of the finite element mesh. To find the contact stiffness accurately, the tip–surface deformation is calculated in FEA and Eq. (A6) is employed. Hence, the relation in Eq. (A1) may not hold.

To use Hertzian theory relations in the CSA, the surface should be modeled by a lumped spring with no loss. In the implementation of the CSA, the frequency is chosen as 100 kHz where the imaginary part of the radiation impedance is very large compared to the real part as depicted in Fig. 2. Hence, this small radiation loss can be neglected and k_S is assumed to be a real number. The calculations indicate that the small loss approximation is valid up to the GHz range.

Table II summarizes the results from three methods. The agreement between the FEA and CSA results and Hertzian theory is within 3% except for the FEA results for the resist

TABLE II. Calculated contact radius, a, and contact stiffness, k, between various tip and half space materials using Hertzian theory, FEA, and the CSA ($F_0=200$ nN, $R=100$ nm).

Material (tip/half space)	Hertzian theory		FEM		CSA	
	a (nm)	k (N/m)	a (nm)	k (N/m)	a (nm)	k (N/m)
Silicon/silicon	5.97	841.7	6.04	849.4	6.05	820.5
Silicon/resist	15.31	128.0	14.85	119.7	15.58	123.7
Silicon/aluminum	6.71	666.7	6.44	664.0	6.85	645.9
Silicon/tungsten	5.19	1113.2	5.23	1120.4	5.26	1083.0

half space. The 7% difference can be reduced by increasing the finite thickness of the soft half space in the FEA. In other words, the FEA calculation is for a finite rather than an infinite half space. One should also note the approximations made in the CSA approach. The radiation impedance calculation neglects the components of stress parallel to the surface and it assumes uniform stress over the contact. Nevertheless, these results verify the adequacy of the FEA implementation and the CSA in determining the contact stiffness.

B. Contact stiffness of layered materials

Quantitative analysis of thin films using the ultrasonic AFM requires understanding of relations between the contact stiffness and thin film properties such as thickness, elastic properties, etc. The CSA provides a natural approach for the evaluation of thin films since any layered material can be included in the calculation through the surface impedance tensor as in Eq. (2.4). Hertzian theory cannot be directly applied to layered materials and the nonlinear contact analysis using FEM suffers from convergence difficulties and it consumes too much computational time and resources.

Different layers on a silicon substrate are evaluated using both the CSA and FEA. Resist, aluminum, and tungsten are chosen as the layer materials. The first two materials can be considered as soft layers on a hard substrate, whereas the last material is an example of a stiff layer on a soft substrate. The properties of the AFM tip are the same as those in Sec. IV.A as is the frequency for the radiation impedance calculation.

Figure 4 depicts FEA and CSA results for aluminum and resist layers on the silicon substrate. For a vanishing layer thickness, the contact stiffness approaches the value that would be obtained for a half space made of the substrate material. On the other hand, when the layer thickness is large compared to the tip dimensions, one obtains the contact stiffness for the tip–layer material half space, which is smaller in the case of resist and aluminum layers on silicon. As expected, the situation is reversed for a tungsten layer on a silicon substrate which is shown in Fig. 5.

These results can be used to quantify the thin film characterization ability of the ultrasonic AFM with regard to film thickness sensitivity and penetration depth. It is assumed that the ultrasonic AFM measures the resonance frequency shifts of a cantilever that are due to contact stiffness changes. This method is shown to be the most sensitive approach for contact stiffness measurements.[3,5,6] The accuracy of the resonance shift measurement, hence determination of the contact stiffness, is limited by the signal to noise ratio (SNR) of the microscope. In this case, the minimum detectable contact stiffness change, Δk, can be considered as a measure of the

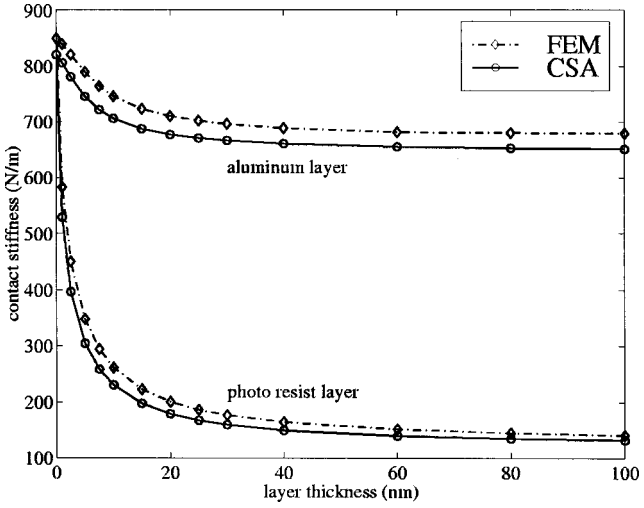

FIG. 4. Calculated surface stiffness using FEA and the CSA. Soft layer (aluminum or photoresist) on a hard substrate (silicon). The frequency for the radiation impedance calculation is chosen as 100 kHz ($F_0=200$ nN, $R=100$ nm).

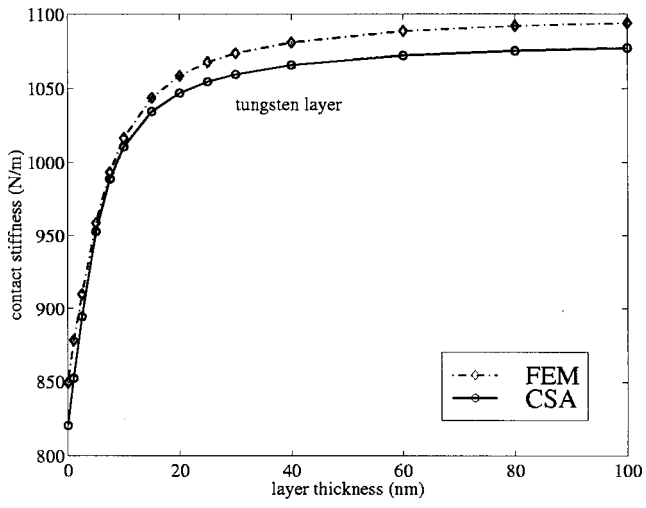

FIG. 5. Calculated surface stiffness using FEA and the CSA. Hard layer (tungsten) on soft substrate (silicon). The frequency for the radiation impedance calculation is chosen as 100 kHz ($F_0=200$ nN, $R=100$ nm).

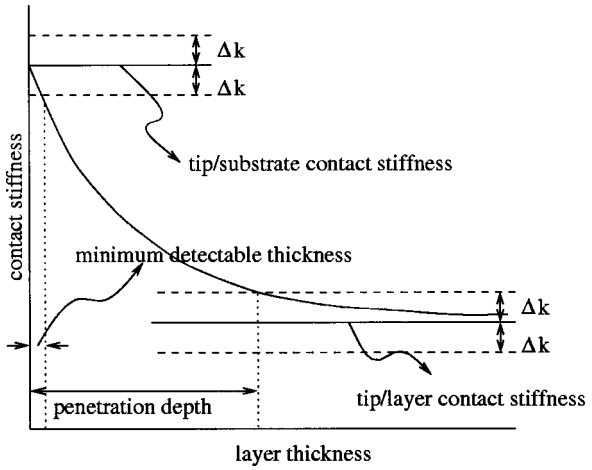

FIG. 6. Definitions of the minimum detectable layer thickness and the penetration depth on a generic curve. The minimum detectable contact stiffness change is denoted by Δk.

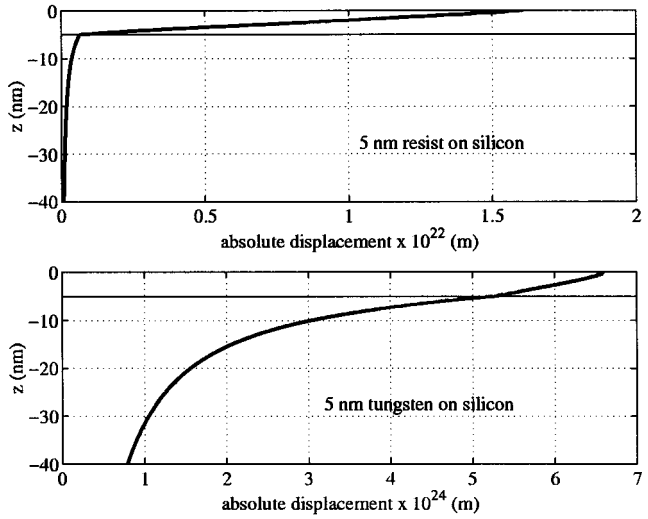

FIG. 7. On axis normal component of the particle displacement into the layered material. The solid lines depict the interface at $z=-5$ nm. Note the two orders of magnitude difference in the displacement scales.

SNR. The main sources of the noise in an ultrasonic AFM (UAFM) system are the mechanical noise of the cantilever, electronics noise, and the shot noise of the laser beam. Besides these noise sources, the accuracy of the resonance shift measurement is also affected by the quality factor and the sensitivity of the cantilever's flexural mode which is being employed by the UAFM. For a given Δk and layer–substrate material pair, the minimum detectable layer thickness and the penetration depth can be defined. The minimum detectable layer thickness (MDLT) is the layer thickness which results in a difference of $\pm\Delta k$ between the measured contact stiffness and that of the tip–substrate half space. The penetration depth is the layer thickness around which the difference between the measured contact stiffness and that of the tip–layer half space is $\pm\Delta k$. It indicates the maximum layer depth the ultrasonic AFM is sensitive to buried layers, interfaces, defects, etc. (see Fig. 6).

From Fig. 6, it is apparent that the MDLT is proportional to the slope of the contact stiffness curve around zero layer thickness. Hence, the ultrasonic AFM is more sensitive when there is a large contrast in the elastic properties of the layer and the substrate in the case of single layered materials. The penetration depth also increases with increasing contrast. Table III summarizes MDLT and penetration depth calculations for different material pairs. In calculating the data in Table III, Δk is chosen as 10 N/m.[16]

Plots of field elastic field distribution in the layered materials also reveal the effect of material property contrast. In Fig. 7, the variation of on axis normal particle displacements under the tip is depicted for 5 nm thick resist and tungsten layers on silicon. The displacement field is concentrated in the resist layer compared with the tungsten layer where the field extends to a greater depth.

It is also possible to calculate the penetration depth as a function of dc force, shown in Fig. 8 where it is assumed that Δk is 10 N/m and the material is a resist layer on a silicon substrate. The penetration depth increases nonlinearly with increasing force, whereas it has a linear relation to the contact radius.

TABLE III. MDLT and penetration depth for different layer materials on a silicon substrate ($F_0=200$ nN, $R=100$ nm, $\Delta k=10$ N/m).

Material	Resist	Aluminum	Tungsten
MDLT (nm)	0.015	0.715	0.248
Penetration depth (nm)	95.75	61.38	66.84

V. CONCLUSION

The layer thickness measurement is crucial in many applications for material characterization. An ultrasonic AFM can determine layer thickness with high resolution through the contact stiffness measurement. In this article, an algorithm for the calculation of the contact stiffness between an AFM tip and layered materials as a function of layer thick-

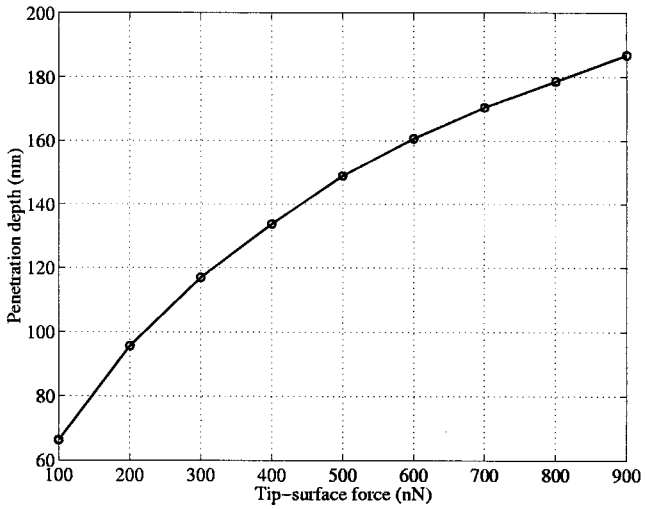

FIG. 8. Maximum detectable layer thickness (penetration depth). It is assumed that the minimum detectable change in the contact stiffness is 10 N/m. The material is resist on a silicon substrate ($R=100$ nm).

ness was described. The algorithm was based on calculation of the radiation impedance seen by a small source resulting from tip–surface contact. The algorithm is very fast and easy to converge compared to FEA. The algorithm, which was verified for half spaces and single layered materials, can be easily extended to the multilayered case.

The radiation impedance method can also be used to calculate the power coupled to the material surface from the AFM tip; this can be significant for large tip radii and high ultrasonic frequencies.

Using the results of the CSA algorithm, the minimum detectable layer thickness and penetration depth were defined. The results indicated that the ultrasonic AFM is more sensitive to the very thin layers and layer–substrate pairs whose elastic properties are very different, which is encouraging for the examination of monolayers and biological films.

As a final remark, the radiation impedance of a surface is also affected by the adhesion properties of the interfaces between layers and the substrate. Hence, it may be possible to detect flaws between layers with this instrument.

ACKNOWLEDGMENT

This work was partially supported by the Office of Naval Research/JSEP.

APPENDIX: HERTZIAN CONTACT EQUATIONS

Hertzian theory defines the contact mechanics between two spherical surfaces. It can also be used to solve contact problems involving a spherical surface and a plane by assuming an infinite radius of curvature for one of the spherical surfaces. This is a case where an AFM tip is pressed upon a sample surface by a force, F_0. The contact radius, a, and stiffness, k, are given by

$$a = \sqrt[3]{\frac{3F_0R}{4E^{*2}}}, \tag{A1}$$

$$k = \sqrt[3]{6F_0RE^{*2}}, \tag{A2}$$

where R is the tip radius. E^* is the effective Young's modulus of the tip–sample contact and is given by

$$\frac{1}{E^*} = \frac{1}{E_T^*} + \frac{1}{E_S^*}, \tag{A3}$$

with

$$E_T^* = \frac{E_T}{1-\rho_T^2}, \quad E_S^* = \frac{E_S}{1-\rho_S^2}, \tag{A4}$$

where E_T^* and E_S^* are the reduced Young's moduli of the tip and the sample, respectively. ρ_T, ρ_S, E_S, and E_T, are the Poisson ratios and the Young's moduli. E_T^* or E_S^* can also be viewed as reduced Young's moduli of the tip–sample contact when the tip is pressed against a rigid sample, i.e., $E_S = \infty$ or the sample is against a rigid tip, i.e., $E_T = \infty$. So it is possible to calculate the contributions of the tip and the sample to the contact separately.

Equations (A1) and (A2) can be combined to obtain a simple relation between the contact radius and the stiffness,

$$a = \frac{k}{2E^*}. \tag{A5}$$

Moreover, deformation is given by

$$h = \frac{3F_0}{2k}. \tag{A6}$$

[1] G. Binnig, C. F. Quate, and Ch. Gerber, Phys. Rev. Lett. **56**, 930 (1986).
[2] U. Rabe and W. Arnold, Appl. Phys. Lett. **64**, 1493 (1994).
[3] P. Variac and B. Cretin, Appl. Phys. Lett. **68**, 461 (1996).
[4] K. Yamanaka, H. Ogiso, and O. Kolosov, Appl. Phys. Lett. **64**, 178 (1994).
[5] U. Rabe, K. Janser, and W. Arnold, Rev. Sci. Instrum. **67**, 3281 (1996).
[6] K. Yamanaka and S. Nakano, Appl. Phys. A: Mater. Sci. Process. **66**, S313 (1998).
[7] L. Landau and E. M. Lifshitz, *Theory of Elasticity* (Pergamon, New York, 1959).
[8] G. S. Kino and C. S. DeSilets, Ultrason. Imaging **1**, 189 (1979).
[9] G. F. Miller and H. Pursey, Proc. R. Soc. London **223**, 521 (1954).
[10] B. V. Honein, A. M. B. Braga, P. Barbone, and G. Herrmann, J. Intell. Mater. Syst. Struct. **2**, 542 (1991).
[11] F. L. Degertekin, B. V. Honein, and B. T. Khuri-Yakub, IEEE Trans. Ultrason. Ferroelectr. Freq. Control (to be published).
[12] F. L. Degertekin, Ph.D. thesis, Stanford University, 1997.
[13] B. A. Auld, *Acoustic Fields and Waves in Solid* (Krieger, Malamar, FA, 1990).
[14] ANSYS, Inc., 201 Johnson Road, Houston, PA 15342-0065.
[15] Following ANSYS nonlinear analysis options autots, lnsrch, and pred have been used.
[16] By using our UAFM setup, we measured the change in the resonance frequency of a particular mode of a silicon cantilever when it is in contact with silicon and photoresist substrates. In this case, 60 kHz change in the resonance frequency corresponds to 714 N/m change in the surface stiffness. The minimum detectable resonance frequency change in our setup is 850 Hz which results in a 10 N/m detectable change in the surface stiffness provided that the tip–sample force is constant.